

# Cyclic Undrained Strength of Sand by Simple Shear Test and Triaxial Test II

(Stress-Strain Conditions in Simple Shear Test)

単純せん断試験と三軸試験による砂の動的非排水強度(II)

Fumio Tatsuoka\*, Marshall L. Silver\*\*,

龍岡 文夫・マーシャル L. シルバー

Apichart Phukunhaphan\*\*\* and Avramidis Anestis\*\*\*\*

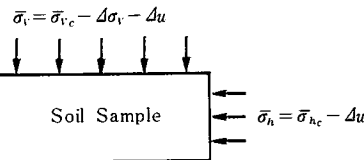
アピチャートフクナフアン・アブラミディス アナスティス

## 5. Stress-Strain Condition in Simple Shear Test

From the time histories as shown in Figs. 2\* and 3\*, the variations of effective vertical stress  $\bar{\sigma}_v$  and effective horizontal stress  $\bar{\sigma}_h$  can be evaluated as illustrated in Fig. 4. The time histories of  $\bar{\sigma}_v$  and  $\bar{\sigma}_h$  at no shear stress during cyclic loading which were obtained from the data shown in Figs. 2 and 3 are shown in Fig. 5. In Fig. 6 is shown effective stress path in terms of  $\bar{\sigma}_v$  and  $\bar{\sigma}_h$  during cyclic loading which was constructed from the values shown in Fig. 5. In this figure, stress points both at no shear stress and at peak shear stress are shown. It can be seen from this figure that there is a unique effective stress path irrespective of the value of shear stress. It can be also seen from this figure that this effective stress path is very similar to that of a  $K_0$  rebound test in which horizontal strain is not allowed during vertical stress is decreased. At the same time, a faster reduction of  $\bar{\sigma}_v$  can be seen than that of  $\bar{\sigma}_h$ . It is obvious that if the equipment was not rigid enough vertically, a reduction of  $\bar{\sigma}_v$  would not have been as fast as seen in Fig. 6. Measured vertical rigidity of the equipment was 0.014 mm for the vertical load of 230 N which induces 60 kN/m<sup>2</sup> in

the vertical stress in a simple shear specimen having the diameter of 7 cm. All these facts described above show that the equipment has an enough vertical rigidity.

From these considerations, it can be concluded that there were no significant vertical and horizontal strains in a simple shear specimen during cyclic undrained tests in this study. These strain conditions are also expected in an in situ soil element in a level ground which is subjected to upward shear wave propagation during earthquake motion.



- $\bar{\sigma}_v$  : Effective Vertical Stress during Cyclic Loading
- $\bar{\sigma}_{vc}$  : Effective Vertical Stress during Consolidation
- $\Delta\sigma_v$  : Change of Total Vertical Stress during Cyclic Loading
- $\sigma_h$  : Effective Horizontal Stress during Cyclic Loading
- $\bar{\sigma}_{hc}$  : Effective Horizontal Stress during Consolidation
- $\Delta u$  : Pore Pressure Development during Cyclic Loading

Fig. 4 Method for evaluating effective vertical stress and effective horizontal stress during cyclic loading.

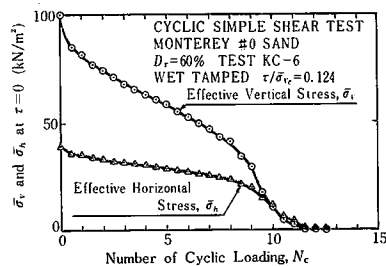


Fig. 5 Relationships between effective vertical stress  $\bar{\sigma}_v$  and effective horizontal stress  $\bar{\sigma}_h$  and number of cyclic loading for wet tamped Monterey No. 0 sand of  $D_r = 60\%$

\* Department of Building and Civil Engineering, Institute of Industrial Science, University of Tokyo.

\*\* Department of Materials Engineering, University of Illinois at Chicago Circle, Chicago, Illinois, USA

\*\*\* Fugro National, Inc. Long Beach, California, USA, Formerly Graduate Student of University of Illinois at Chicago Circle

\*\*\*\* Commonwealth Gilbert, Jackson, Michigan, USA, Formerly Graduate Student of University of Illinois at Chicago Circle

\* See Tatsuoka et al (1981), "Cyclic Undrained Strength of Sand by Simple Shear Test and Triaxial Test I," Seisan Kenkyu Vol. 32, No. 1.

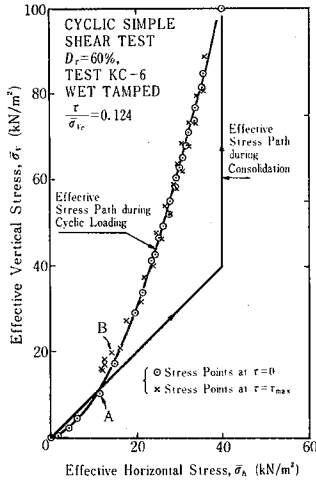


Fig. 6 Effective stress path for wet tamped Monterey No. 0 sand of  $D_r = 60\%$  (Refer to Fig. 3 for points A and B)

Therefore, the effective stress condition in a cyclic simple shear specimen can be considered very similar to that of the in situ soil element. However, it should be noted that total stress condition in a cyclic simple shear specimen during cyclic loading in this study is not exactly identical to that of an in situ soil element. The difference involves the variations in total vertical stress and in total horizontal stress. These are illustrated in Figs. 7 and 8. For this reason, measured excessive pore pressure in cyclic simple shear test in this study is less than excessive pore pressure under the similar in situ condition.

The relationship between double amplitude shear strain  $DA$  in percentage and number of cyclic loading  $N_c$  which was obtained from the data shown in Fig. 2\* is shown in Fig. 9. Numbers of cyclic loading where  $DA$  became 1.5%, 3%, 7.5% and 15% were read from this relationship for each test as illustrated in Fig. 9.

Similar test results which were obtained from tests on wet tamped specimens of  $D_r = 45\%$  and  $80\%$  are shown in Figs. 10 through 15. Three features should be noted.

(a) Similar effective stress paths during cyclic undrained loading as shown in Figs. 6, 11 and 14 can be seen for different densities.

(b) As seen from Fig. 10, effective stress in a sample of  $D_r = 45\%$  can easily become zero after the rate of decrease in effective stress increases (this is after number of cyclic loading of 5 in the case of Fig. 10). Therefore, it is practically easy to define the moment of initial liquefaction for a sample of  $D_r = 45\%$ . On the other hand, as seen from

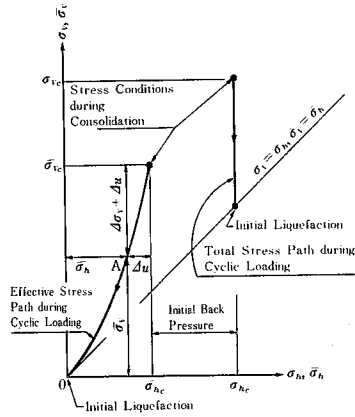


Fig. 7 Total and effective stress paths in cyclic simple shear test in this study.

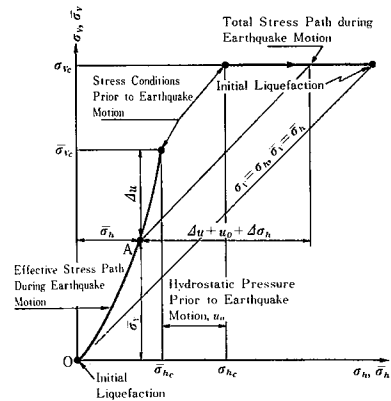


Fig. 8 In situ total and effective stress paths during earthquake motion.

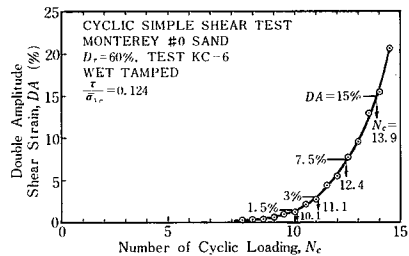


Fig. 9 Relationship between double amplitude shear strain and number of cyclic loading for wet tamped Monterey No. 0 sand of  $D_r = 60\%$

13, effective stress in a sample of  $D_r = 80\%$  does not become zero as rapidly as in a looser sample. Therefore, it is difficult to define clearly the moment of initial liquefaction for a sample of  $D_r = 80\%$ .

(c) As seen in Fig. 12, shear strain increases rapidly after initial liquefaction in a sample of  $D_r = 45\%$ . However, as seen in Fig. 15, shear strain does not increase rapidly even

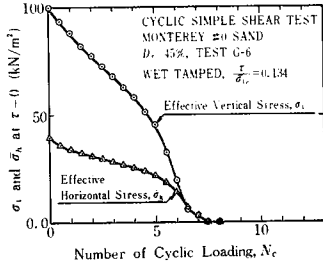


Fig. 10 Relationships between effective vertical stress and effective horizontal stress and number of loading for wet tamped Monterey No. 0 sand of  $D_r = 45\%$

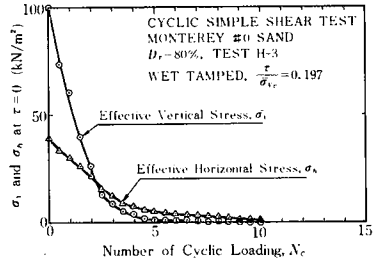


Fig. 13 Relationships between effective vertical stress and effective horizontal stress and number of cyclic loading for wet tamped Monterey No. 0 sand of  $D_r = 80\%$

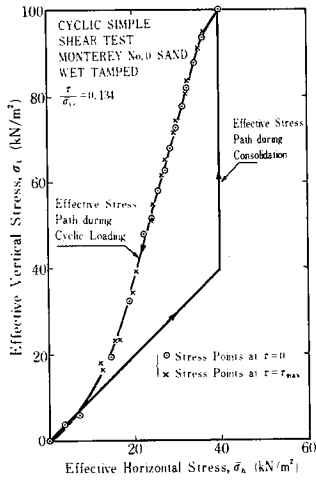


Fig. 11 Effective stress path for wet tamped Monterey No. 0 sand of  $D_r = 45\%$

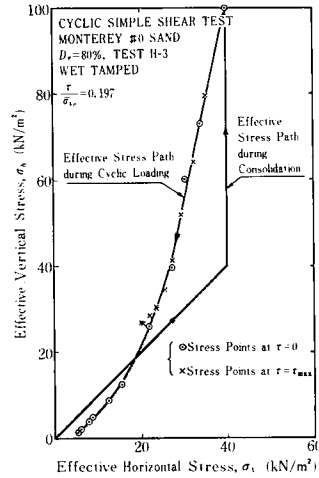


Fig. 14 Effective stress path for wet tamped Monterey No. 0 sand of  $D_r = 80\%$

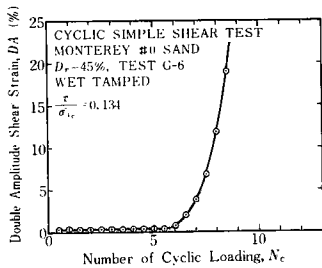


Fig. 12 Relationship between double amplitude shear strain and number of cyclic loading for wet tamped Monterey No. 0 sand of  $D_r = 45\%$

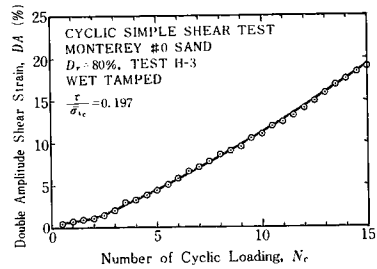


Fig. 15 Relationship between double amplitude shear strain and number of cyclic loading for wet tamped Monterey No. 0 sand of  $D_r = 80\%$

after initial liquefaction in a sample of  $D_r = 80\%$ . This means that while shear strain after initial liquefaction is almost unlimited in a sample of  $D_r = 45\%$ , limited shear strain is expected in a sample of  $D_r = 80\%$  even if initial liquefaction has been observed.

The relationship between the normalized stress ratio  $\tau/\sigma'_v$ , in which  $\tau$  is the amplitude of cyclic shear stress and

$\sigma'_v$  is consolidation effective vertical stress induced by the test and the numbers of cyclic loading  $N_c$  to initial liquefaction, 1.5%, 3%, 7.5% and 15% double amplitude shear strains is shown for wet tamped specimens of  $D_r = 60\%$  in Fig. 17. Numbers of cyclic loading at which a certain value of shear strain amplitude is induced or the state of initial liquefaction is observed increases with decreasing stress ratio

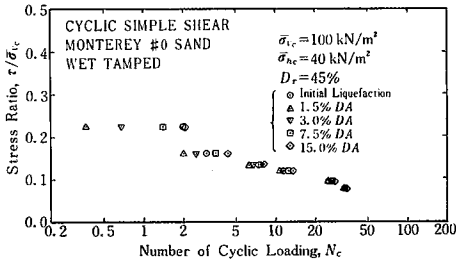


Fig. 16 Stress ratio versus number of cyclic loading to initial liquefaction, 1.5%, 3%, 7.5% and 15% double amplitude shear strains for wet tamped specimens of  $D_r = 45\%$

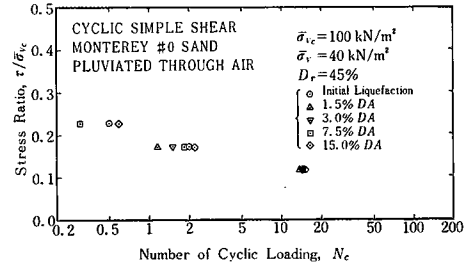


Fig. 19 Stress ratio versus number of cyclic loading to initial liquefaction, 1.5%, 3%, 7.5% and 15% double amplitude shear strains for air pluviated specimens of  $D_r = 45\%$

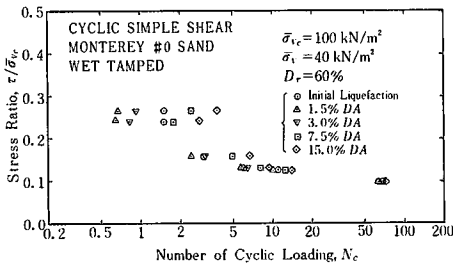


Fig. 17 Stress ratio versus number of cyclic loading to initial liquefaction, 1.5%, 3%, 7.5% and 15% double amplitude shear strains for wet tamped specimens of  $D_r = 60\%$

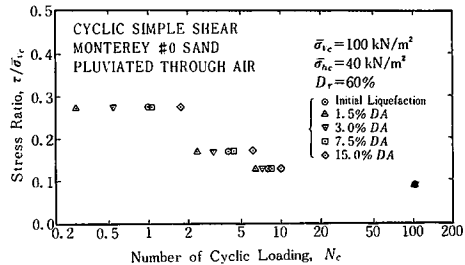


Fig. 20 Stress ratio versus number of cyclic loading to initial liquefaction, 1.5%, 3%, 7.5% and 15% double amplitude shear strains for air pluviated specimens of  $D_r = 60\%$

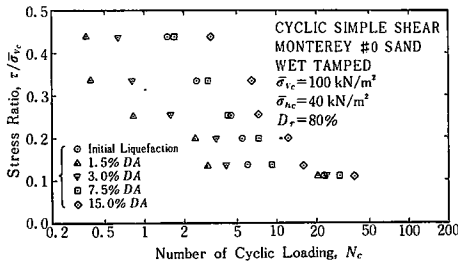


Fig. 18 Stress ratio versus number of cyclic loading to initial liquefaction, 1.5%, 3%, 7.5% and 15% double amplitude shear strains for wet tamped specimens of  $D_r = 80\%$

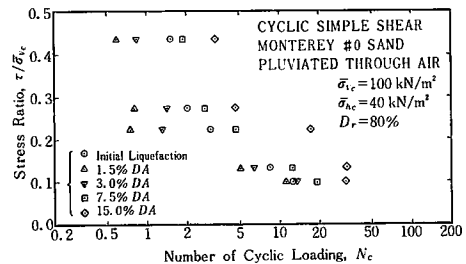


Fig. 21 Stress ratio versus number of cyclic loading to initial liquefaction, 1.5%, 3%, 7.5% and 15% double amplitude shear strains for air pluviated specimens of  $D_r = 80\%$

$\tau/\sigma'_{vc}$ . Similar results for wet tamped specimens of  $D_r = 45\%$  and  $80\%$  are shown in Figs. 16 and 18, respectively. Also shown in Figs. 19, 20 and 21 are test results of specimens pluviated through air of  $D_r = 45\%$ ,  $60\%$  and  $80\%$ ,

respectively. These data will be analyzed to compare with cyclic undrained triaxial data in the following.

(to be continued)

(Manuscript received, November 8, 1979)